

Changes in the fractal dimension on pre- and post-implant panoramic radiographs

Kaustubh Sansare · Dharamveer Singh ·
Freny Karjodkar

Received: 8 June 2011 / Accepted: 25 September 2011 / Published online: 1 November 2011
© Japanese Society for Oral and Maxillofacial Radiology and Springer 2011

Abstract

Objectives The aim of this study was to assess the changes in the fractal dimension before and after implant placement. The study also examined the possibility of using fractal analysis as a prognostic indicator for implant success.

Methods Pre- and post-implant panoramic radiographs of 33 patients who underwent implant treatment were archived. Square regions of interest were cropped, and a fractal analysis was performed using the box-counting method of ImageJ 1.42 software.

Results The Wilcoxon test revealed a significant difference between the pre- and post-implant values. This difference could indicate an increased bony microstructure around the implant, thereby aiding the prediction of implant success.

Conclusions The increase in the fractal analysis values suggests increased bony microstructure in the peri-implant sites after implant placement. Consensus on the technique of evaluating fractal analysis and further experimental studies could render fractal analysis a prognostic indicator for implant success.

Keywords Fractal analysis · Implant · Panoramic radiograph

Introduction

The concept of fractal analysis was first introduced by Mandelbrot [1]. The term fractal is derived from the Latin adjective *fractus*, which means broken. Mandelbrot identified familiar shapes, curves, surfaces, disconnected dust, and odd shapes using fractal analysis. Researchers have used fractal analysis in describing and measuring the morphology of the natural world. For example, fractal analysis has been applied to describe dripping taps, stock exchange prices, cell outlines, pulmonary branching, heart beats, and temporomandibular joint sounds [2, 3]. Since the publication of *The Fractal Geometry of Nature* by Mandelbrot in 1983, medical radiologists have used fractal analysis as an indicator of bone changes that are independent of variables such as projection geometry, alignment, and radiodensity [4–6].

There is a popular opinion that the internal structure of cancellous bone is determined by the functional load on the bone. Trabeculae do not always intersect at right angles, and minimizing stress does not appear to be the most important goal in bone remodeling [7, 8].

Some researchers have already suggested that fractal analysis of alveolar trabecular bone could be used as a diagnostic tool to objectively characterize alveolar bone [9] and may be a sensitive descriptor in bone studies [10]. It has been established that cancellous alveolar bone is composed of interconnected trabecular structures with an underlying geometric pattern, thus making it a tool for defining a mathematical fractal pattern [11]. Despite the establishment of many methods to investigate the quality of alveolar bone, fractal analysis of bone has the potential to be the most popular because it is an accurate, economical, and readily available method. Many attempts have been made to predict and analyze trabecular bone using fractal analysis [12–15].

K. Sansare (✉) · D. Singh · F. Karjodkar
Oral Medicine and Radiology, Nair Hospital Dental College,
Mumbai, India
e-mail: kaustubhsansare@yahoo.com

D. Singh
e-mail: drdsingh@gmail.com

F. Karjodkar
e-mail: fkarjodkar@yahoo.co.in

The key factors for success of implants are a series of patient-related and procedure-dependent parameters, including general health, biocompatibility, implant material, microscopic and macroscopic structures of the implant surface, and quality and quantity of the alveolar bone [16]. The response of bone to placement of an implant is of crucial importance for the prognosis of the implant.

A minimum period of 3–6 months of healing is required after implant placement before the implant is loaded [17]. The implant then becomes osseointegrated as part of the mechanical continuum of the alveolar bone without the buffer of the periodontal ligament space. The fractal nature of the trabecular pattern of alveolar bone can be at least partially characterized by the fractal dimension (FD) [18]. Mechanical integration of the implant-bone interface provides unique opportunities to study the response of alveolar bone trabeculae to implant placement. Therefore, it was decided to test our hypothesis that placement of an implant changes the orientation of the bony trabeculae.

This study was undertaken to examine the trabecular changes taking place in the alveolar bone on panoramic radiographs before and after implant placement. The study also examined the possibility of using these changes as a prognostic indicator for implant success.

Materials and methods

This study was submitted to and approved by the local Institutional Review Board of Nair Hospital Dental College on 18 December 2009. Panoramic radiographs of 50 patients who had received intraosseous implants were retrieved from the archives of the oral and maxillofacial radiology unit of Nair Hospital Dental College, Mumbai, India, and a private implant center also based in Mumbai.

Two panoramic radiographs, namely the pre- and post-implant radiographs, were retrieved for the 50 patients. The inclusion criteria were any patient who had both panoramic radiographs available, with the pre-implant radiograph taken on the day of implant placement and the post-implant radiograph taken 3 months after the implant placement. The exclusion criteria included implant placed in the anterior region, implant placed in areas of bone graft, implant placed after sinus lift surgery, immediate implant placement after extraction, or immediate loading of implants.

In view of these criteria, 33 patients (20 males, 13 females, mean age 55 years, age range 25–70 years) were finally selected for this study. A total of 50 implant sites were studied in the 33 patients. Of the 50 implant sites, 23 were in the maxilla and 27 were in the mandible. All the implants were placed using the two-step surgical protocol described by Branemark [17].

All panoramic radiographs were obtained using a Kodak digital 9000 panoramic unit (Carestream Health, Rochester, NY, USA) with parameters of 72–80 kVp, 8–12 mA, and 18-s exposure time. The panoramic radiographs were taken in the standing position, and the patients were asked to bite on the biting portion of the radiographic equipment using the anterior teeth to establish the location. The Frankfort horizontal plane was placed parallel to the horizontal plane to maintain a consistent head position. The sensor matrix was $61 \times 1,244$ pixels, and the image size was 18×24 cm. A 14-bit image was obtained, with 16,384 gray scales. The sensor technology used was a charge-coupled device–optical fiber sensor with a cesium iodide coating. All original digital imaging and communications in medicine (DICOM) images were transferred to a separate workstation, and a square region of interest (ROI) was placed on the distal aspect of the peri-implant area on the post-implant radiographs. One side of the square was oriented parallel to the long axis of the implant, without including any part of the implant in the ROI. The other side was placed at the level of the apical end of the implant. Another square ROI was placed in a similar region on the pre-implant radiograph (Fig. 1). Two observers with a minimum of 5 years of experience in maxillofacial radiology were appointed to place the ROIs and assess the FD. Both observers underwent training until they were comfortable with the ROI placement and FD assessment.

The intraobserver agreement in the ROI placement was assessed by having the same observer view all the images twice, with a 3-week interval between the viewings. The interobserver reliability was assessed by having the two observers place the ROIs and assess the FD separately. The ROIs were cropped and used for fractal analysis. All ROIs were selected on the images as squares of 80×80 pixels. All ROIs were outlined on the radiographs using Adobe Photoshop CS3 (Adobe Systems, San Jose, CA, USA). The ROIs were selected from the apical end of the implant to prevent any influence of alterations from the crestal bone after implant placement.

Fractal analysis was performed using ImageJ 1.42 software, as a version of NIH Image (US National Institutes of Health, <http://rsb.info.nih.gov/nih-image>). NIH Image is a public domain program that was downloaded from the Internet (<http://rsb.info.nih.gov/ij/download.html>) on 9 November 2009 using Java 1.6.0_10.

The saved images were processed for the FD analysis using the box-counting method proposed in a previous report [19]. The cropped image was duplicated, and the duplicated image was blurred with a Gaussian filter (kernel size 30) to remove medium and fine scale variations in the image brightness. The blurred image was then subtracted from the original image, and 80 was added to the resultant image at each pixel location. The blurring, subtracting, and

Fig. 1 ROIs selected as squares of 80×80 pixels on pre- and post-implant radiographs

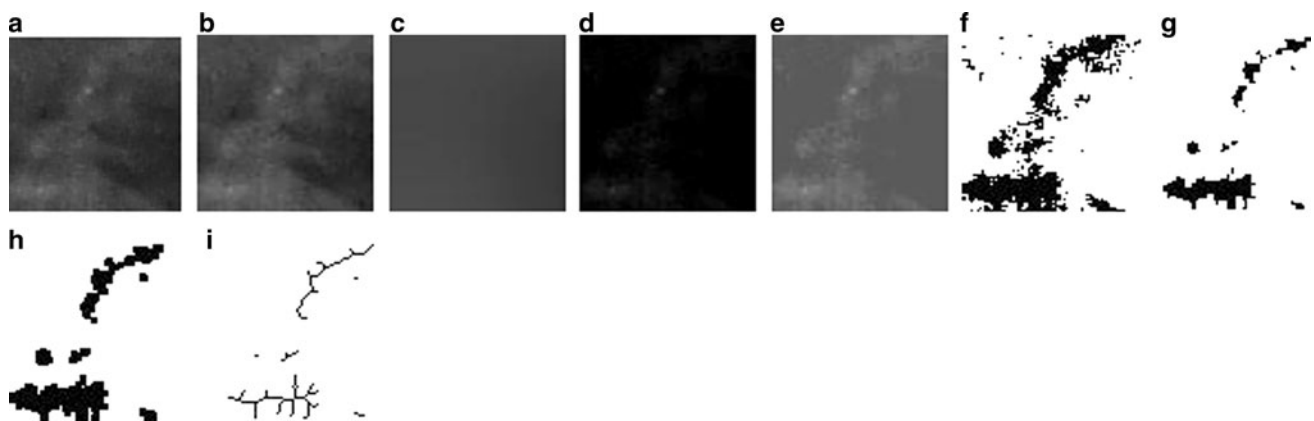
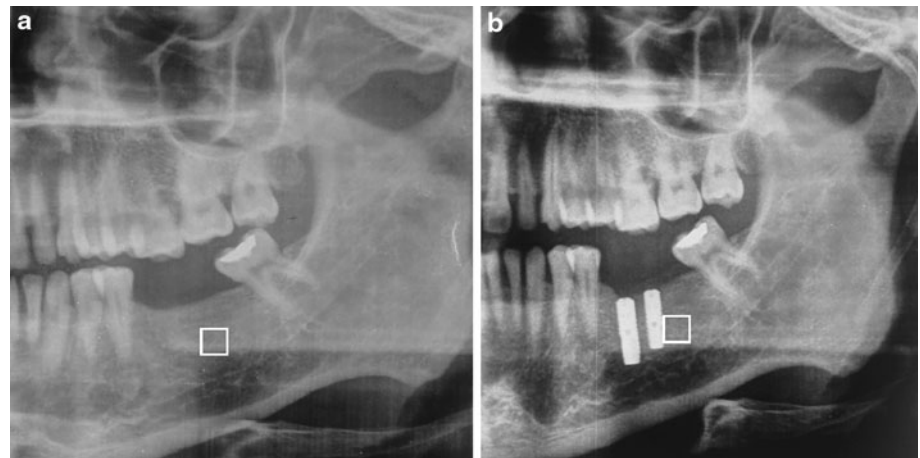


Fig. 2 Different steps involved in calculating the FD from a pre-implant radiograph. **a** Cropped ROI transferred to ImageJ, **b** duplicated 8-bit image, **c** blurred image, **d** subtracted image, **e** image with added 80, **f** image made binary, **g** eroded image, **h** dilated image, **i** skeletonized image

adding 80 finally resulted in a standard low frequency noise image. The addition of 80 was also performed to obtain the mean gray level of the ROI image. The mean gray level of the ROI image was thus standardized to 80. The image was then made binary with a threshold at a gray value of 80. This resulted in segmental objects approximating the bony trabecular pattern. The binary image was finally eroded and dilated once to remove noise before skeletonization. The final image was then ready for fractal analysis (Fig. 2). The skeletal binary image exhibited a skeletal structure representing the bone pattern and a nonskeletal pattern representing the bone marrow [20]. The FD was calculated using the box-counting method from the “analyze” menu. The image was initially covered by a square grid of equally sized tiles, and the number of tiles referring to the trabecular bone was counted. The widths of the boxes were 2, 3, 4, 6, 8, 12, 16, 32, and 64 pixels. The number of counted tiles was then plotted against the size of the box on a double logarithmic scale. The slope of the line fitted to the data points finally represented the FD (Fig. 3). The same

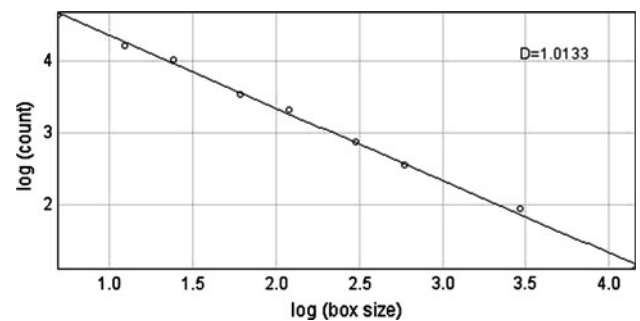


Fig. 3 Slope of the line fitted to the data points along with the FD value for the pre-implant radiograph of the same patient represented in Fig. 2

procedure was repeated to calculate the FD for the post-implant radiographs (Figs. 4, 5).

Since parametric tests failed, a nonparametric test was applied for the intraobserver agreement and interobserver reliability. The intraobserver agreement and interobserver reliability were evaluated by Cronbach’s alpha, where an

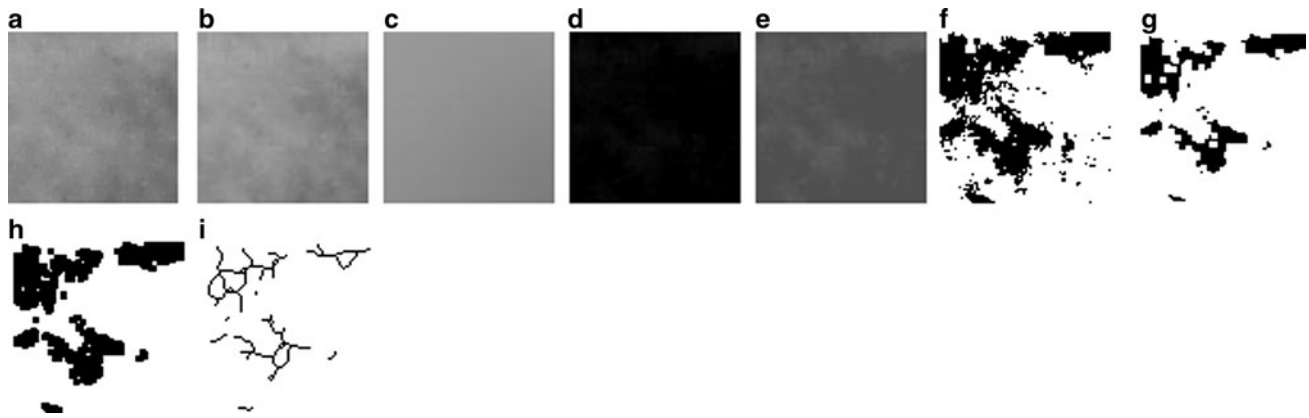


Fig. 4 Different steps involved in calculating the FD from the post-implant radiograph of the same patient represented in Figs. 2 and 3. **a** Cropped ROI transferred to ImageJ, **b** duplicated 8-bit image,

c blurred image, **d** subtracted image, **e** image with added 80, **f** image made binary, **g** eroded image, **h** dilated image, **i** skeletonized image

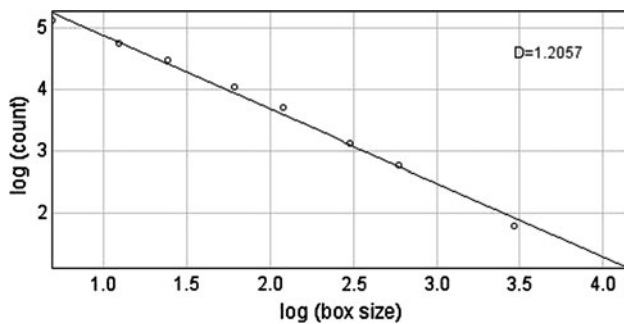


Fig. 5 Slope of the line fitted to the data points along with the FD value for the post-implant radiograph of the same patient represented in Figs. 2 and 3

alpha value of 0.8 or greater was considered to constitute agreement or reliability, respectively.

Results

The 33 patients enrolled in this study comprised 20 males and 13 females, who ranged in age from 25 to 71 years. Among the 33 patients, 3 patients had decreased FD values on their post-implant radiographs.

Observer one

For observer one, the FD values of all 33 cases ranged from 0.009 to 1.335 on the pre-implant radiographs and from 0.842 to 1.456 on the post-implant radiographs in session one. In session two, the FD values ranged from 0.604 to 1.357 on the pre-implant radiographs and from 0.846 to 1.372 on the post-implant radiographs.

For session one, the FD analysis of the pre-implant radiographs gave a mean of 0.991, median of 1.015, and standard deviation (SD) of 0.252, while that of the post-

Table 1 Significant difference between the pre- and post-implant FD values for observer one in session one

Variable	Number	Mean	Median	SD	W (Wilcoxon value)
Pre-implant FD	50	0.991	1.015	0.252	1,169 ($p < 0.001$); difference is significant
Post-implant FD	50	1.183	1.164	0.168	

Table 2 Significant difference between the pre- and post-implant FD values for observer one in session two

Variable	Number	Mean	Median	SD	W (Wilcoxon value)
Pre-implant FD	50	1.018	1.06	0.259	118 ($p < 0.001$); difference is significant
Post-implant FD	50	1.203	1.19	0.174	

implant radiographs gave a mean of 1.183, median of 1.164, and SD of 0.168 (Table 1). The nonparametric Wilcoxon signed rank test revealed a significant difference between the pre-implant and post-implant FD values ($p < 0.001$) for session one.

In session two, the FD analysis of the pre-implant radiographs gave a mean of 1.018, median of 1.06, and SD of 0.259, while that of the post-implant radiographs gave a mean of 1.203, median of 1.19, and SD of 0.174 (Table 2). The Wilcoxon signed rank test showed a significant difference between the pre- and post-implant FD values ($p < 0.001$) for session two.

Table 3 Significant difference between the pre- and post-implant FD values for observer two

Variable	Number	Mean	Median	SD	W (Wilcoxon value)
Pre-implant	50	0.976	1.01	0.286	126 ($p < 0.001$); difference is significant
Post-implant	50	1.242	1.11	0.303	

Observer two

For observer two, the FD values on the pre-implant radiographs ranged from 0.383 to 1.298, with a mean of 0.976, median of 1.01, and SD of 0.286, while those on the post-implant radiographs ranged from 0.718 to 1.944, with a mean of 1.242, median of 1.11, and SD of 0.303 (Table 3). The Wilcoxon signed rank test showed a significant difference between the pre- and post-implant values ($p < 0.001$).

Intraobserver agreement

For observer one, the Cronbach’s alpha of the pre-implant radiographs for sessions one and two was 0.986, while that for the post-implant radiographs for sessions one and two was 0.849.

Interobserver reliability

The Cronbach’s alpha values of the pre- and post-implant radiographs were 0.936 and 0.906, respectively, for observer one session one and observer two. The Cronbach’s alpha values of the pre- and post-implant radiographs were 0.916 and 0.956, respectively, for observer one session two and observer two.

There were high alpha values for the intraobserver agreement and interobserver reliability in the ROI placement and FD analysis.

The Bland and Altman model, a coefficient for variation, was used to measure the variability in the interobserver FD values. Bland and Altman plots were constructed for comparisons of the pre- and post-implant FD values between the two observers. The plots indicated SDs of ± 0.5 for the pre-implant radiographs and ± 0.3 for the post-implant radiographs between observers one and two (Fig. 6a, b). The mean absolute differences in the pre- and post-implant FD values for the two observers were within the bounds of the 5% confidence interval.

Age group variations

The 33 patients were divided into five age groups (Table 4). The Kruskal–Wallis one-way analysis test was

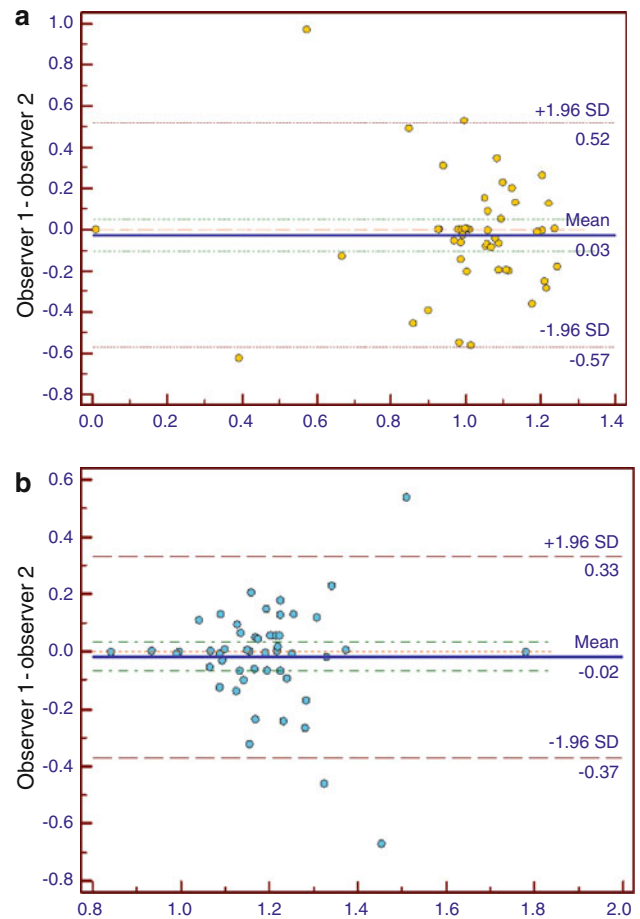


Fig. 6 Bland and Altman plots showing the interobserver variability in the FD values between observers one and two. **a** Average pre-implant FD values for observers one and two. **b** Average post-implant FD values for observers one and two

Table 4 Kruskal–Wallis one-way analysis of variance for various age groups

Age (years)	Number	Mean	Median	SD
24–34	3	0.75	0.99	0.66
35–44	3	1.10	1.10	0.11
45–54	8	1.03	1.02	0.16
55–64	9	1.06	1.06	0.15
65–74	10	0.93	1.02	0.36

applied to data obtained from session one of observer one to compare the pre- and post-implant FD values in different age groups. The Kruskal–Wallis test revealed medians ranging from 0.008 to 0.16 for all five age groups. The difference between the pre- and post-implant FD values for the different age groups was not significant ($p = 0.900$).

Table 5 Significant difference between the pre- and post-implant FD values for the maxilla

Maxilla	Number	Mean	Median	SD	W (Wilcoxon value)
Pre-implant FD	23	0.99	1.017	0.24	204 ($p < 0.001$); difference is significant
Post-implant FD	23	1.17	1.137	0.17	

Table 6 Significant difference between the pre- and post-implant FD values for the mandible

Mandible	Number	Mean	Median	SD	W (Wilcoxon value)
Pre-implant FD	27	1.03	1.057	0.27	344 ($p < 0.001$); difference is significant
Post-implant FD	27	1.23	1.194	0.18	

Anatomic variations

Of the 50 implant sites assessed, 23 were in the maxilla and 27 were in the mandible. Only posterior region implant sites were selected for this study to avoid faulty results caused by cervical spine superimposition. The anatomic variations for the maxilla and mandible were analyzed from the data for session one of observer one.

In the maxilla, the FD values for the pre-implant radiographs ranged from 0.604 to 1.293, with a mean of 0.99, median of 1.017, and SD of 0.24, while those for the post-implant radiographs ranged from 0.936 to 1.782, with a mean of 1.17, median of 1.137, and SD of 0.17. The Wilcoxon signed rank test showed a significant difference between the pre- and post-implant FD values ($p < 0.001$) for the maxillary radiographs (Table 5).

In the mandible, the FD values for the pre-implant radiographs ranged from 0.007 to 1.335, with a mean of 1.03, median of 1.057, and SD of 0.27, while those for the post-implant radiographs ranged from 0.846 to 1.556, with a mean of 1.23, median of 1.194, and SD of 0.18. The Wilcoxon signed rank test showed a significant difference between the pre- and post-implant FD values ($p < 0.001$) for the mandibular radiographs (Table 6).

Discussion

Mathematically constructed fractals are known to possess self-similarity. Conversely, biological or natural fractals tend to differ in their characteristics. Since its inception, the

FD has been found to be associated with changes in the bony microstructure. These changes have been observed for various clinical conditions, such as increased load to osteoarthritic knee joints [21], and after immobilization of the heel [22]. The FD has also been found to reflect partial demineralization of bone [23]. Several studies have demonstrated loss of bone mass as a result of decreased function and positive responses of bone to optimal stress [24–29].

The responses of bone to an implant play a pivotal role in the prognosis of the implant. This study was conducted to assess the bone-implant interface for changes in the trabecular pattern. It was hypothesized that placement of an implant leads to a change in the orientation of the bony trabeculae. This hypothesis was proposed because the diameter of a drilled implant osteotomy is usually smaller than the diameter of the inserted implant. Consequently, while tightening of the implant is carried out, broken trabecular fragments could get approximated and come to lie closer to one another, thereby leading to increased bone microstructure.

There are various published techniques for calculating the FD, including the caliper, box-counting, and power spectral methods [13, 30]. We chose the box-counting method of the ImageJ 1.42 software because it was readily available and easy to use.

A previous study found a greater magnitude and occurrence of bone loss during the first year after placement of an implant measuring 1.2 mm with a range of 0–3 mm [31]. Another study reported an average first year bone loss of 0.93 mm, with a range of 0.4–1.6 mm [32]. Early crestal bone loss has been observed so frequently that the proposed criteria for successful implants often do not include the first year bone loss [33]. It was therefore decided not to include the crestal bone in the ROI.

The ROI was placed near the apical end of the implant. Care was taken to avoid inclusion of any part of the implant or anatomic structures such as the inferior alveolar canal, mental foramen, or inferior border of the maxillary sinus in the ROI. Previous studies have suggested that the ROI location is more critical for fractal analysis than its size [34, 35]. A square of 80 × 80 pixels was selected as an ROI because that was the most convenient dimension for placement in the peri-implant area. The ROI placement and FD assessment on the pre-implant radiographs were considered to be controls and compared with those on the post-implant radiographs. The ROI placement and FD assessment could not have been performed on the contralateral side because the contralateral side was not always edentulous. Moreover, biological fractals are not known to be self-similar, unlike mathematical fractals.

The interobserver variation was assessed by appointing two observers for the FD analysis. The intraobserver variation was evaluated by re-placement of the ROI by the

same observer after a 3-week interval in both the pre- and post-implant radiographs. The FD values obtained from observer one during sessions one and two for both the pre- and post-implant radiographs were analyzed by Cronbach's alpha. The high intraobserver and interobserver alpha values found in the present study demonstrate excellent intraobserver agreement and interobserver reliability in the reproducibility of the ROI placement. It should be noted that the factors determining observer agreement may be related to observer experience, radiographic quality, viewing conditions, study design, and study material. The Bland and Altman plots suggested that there was good agreement for the pre- and post-implant FD value measurements between the two observers.

It has been acknowledged in the literature that the FD values from projection X-rays are likely to differ from those derived from cross-sectional images [36]. Two-dimensional radiographs have been shown to contain information about the bone mineral density and trabecular architecture [23]. However, although periapical radiographs can allow for accurate observation and analysis of the fractal pattern, panoramic radiographs have largely been used to determine the FD.

Panoramic radiographs with implant placement have been used for fractal analysis in a previous study [37]. Fractal analysis has also been performed on both periapical and panoramic radiographs, with significant results obtained on both types of images [38]. It has also been concluded that the FD can be calculated from nonstandardized clinical radiographs using different methods [39, 40]. Panoramic radiographs were used in our study to determine the FD because these were routinely advised as pre- and post-implant radiographs as an institutional protocol.

The FD has been used for assessment of osteoporosis, bony healing, and differentiating gingivitis, periodontitis, and normal conditions in healthy adults on dental radiographs [13, 36, 41]. The FD has also been used to differentiate between the occlusal forces in dentulous and edentulous arches [42, 43]. It has also been reported that the FD increases during the bone-healing process [44].

It is still debatable whether a decreasing bone density removes fine trabecular structures by increasing the number of abrupt and erratic density changes with an increased FD or whether a decreasing density eliminates larger interconnecting trabecular struts with a decreased FD [23, 45]. Although most of the earlier studies suggested that a decreasing FD implies decreased bone density [9, 36, 37, 46], there have been conflicting reports in the literature [5, 23].

Dense bone tends to attract strain and become denser. The density of bone is also directly related to the strength of bone [47, 48], and fine trabecular bone is less dense than coarse trabecular bone [49]. There have been reports of

implants appearing to generate bone around themselves [50, 51].

It has already been acknowledged that all fractal analysis studies are fraught with parameters that are difficult to control [52]. It has also been accepted that different methods used for estimation of the FD may not agree in their results, and this remains a gray area with no acceptable universal answer at the present time [46]. However, it has been proposed that the FD may differ because of differences in the anatomy of subjects and the experimental design [16].

In this study, the FD was examined on 33 panoramic radiographs and 50 implant sites before and after implant placement. The FD calculated for the pre-implant radiographs was compared with that for the post-implant radiographs. A nonparametric test, the Wilcoxon signed rank test, was applied because parametric tests failed on these data. The FD value was significantly increased after implant placement for both sessions of observer one and between observers one and two. This consistent increase in the post-implant FD could suggest an increased amount of bony microstructure and bony trabeculae around the implant, thereby making the implant firm and stable. A firm and stable implant could be considered as an early sign of a successful implant [16].

The radiographs of three subjects had significant negative regression slopes, with decreased post-implant FD values, which could be an early sign of failed implants. On follow-up, it was found that the implant treatment had failed in these three patients. Of the three failed implants, two were in the mandible and one was in the maxilla. Implants were considered to have failed if any one or more of the following was present [53]: pain on palpation, percussion, or function; horizontal mobility of more than 0.5 mm; vertical mobility of any degree; radiographic bone loss of more than 4 mm; probing depth of more than 7 mm; presence of uncontrolled exudate; or implant no longer in the mouth.

One of the key factors determining long-term success of an implant is the nature of the bony microstructure around the implant [54]. Bone biopsies have been performed to evaluate the bone quality through histomorphometric analysis [55, 56]. Commonly, X-ray evaluation is used to determine the bone quality. Computed tomography [57, 58] or dual photon X-ray absorptiometry [59] has been used to measure the bone density. In the present study, a fractal analysis was used to evaluate the bony trabeculae around the implants because fractal analysis is easy to perform and readily available. Successful implants are known to generate bone around themselves, thereby increasing their stability quotient in the bone [16, 50, 51, 54]. In our study, a significant increase was observed in the post-implant FD values, suggestive of increased bony trabeculae around the

implants. It can therefore be proposed that fractal analysis may be a useful tool for predicting the prognosis of an implant.

The 33 patients were also divided into five age groups. Most of our patients were placed in the age groups of 55–64 and 65–74 years. The Kruskal–Wallis one-way analysis test was applied to the data obtained from session one of observer one to evaluate the differences between the various age groups for the pre- and post-implant radiographs. It was found that age was not a significant factor for the difference between the pre- and post-implant FD values. This indicates that the pre- and post-implant FD values were not influenced by age. Therefore, it can be concluded that differences in the pre- and post-implant FD values will be observed irrespective of the age of the patient at the time of implant placement.

Of the 50 implant sites analyzed, 23 were in the maxilla and 27 were in the mandible. There were significant differences between the pre- and post-implant FD values for both the maxillary and mandibular sites using the data from session one of observer one. Therefore, it can be concluded that the anatomic site was not a significant factor in the changes in the FD values.

Our findings are also consistent with the only similar study reported [41], which found an increased FD for 2 years after implant placement in 34 implant sites from 18 panoramic radiographs. The findings of this study therefore support the findings of the earlier study.

For fractal analysis to be a routine clinical procedure, there needs to be a consensus on the method of fractal analysis estimation. This could be achieved by conducting more clinical trials and on larger sample sizes. Given the controversy surrounding fractal analysis, there is a need for further analytical clinical studies. This study could form the basis for further studies with different population groups, eventually rendering the FD as a prognostic tool for intraosseous implants.

Acknowledgments The authors would like to acknowledge the following for their contributions to this study and manuscript: Dr. Kiran Kelkar, private implantologist; Dr. Neha Patil, resident, Oral and Maxillofacial Radiology, Nair Hospital Dental College; and, Dr. Abhiram Kasbe, Associate Professor, Preventive and Social Medicine, BYL Nair Hospital and TN Medical College.

References

- Mandelbrot BB. The fractal geometry of nature. 1st ed. New York: WH Freeman; 1983.
- Weibel ER. Fractal geometry: a design principle for living organisms. *Am J Physiol*. 1991;261:L361–9.
- Badwell RSS. The application of fractal dimensions to temporomandibular joint sounds. *Comput Biol Med*. 1993;23:1–4.
- Buckland-Wright JC, Lynch JA, Rymer J, Fogelman I. Fractal signature analysis of macroradiographs measures trabecular organization in lumbar vertebrae of postmenopausal women. *Calcif Tissue Int*. 1994;54:106–12.
- Lynch JA, Hawkes DJ, Buckland-Wright JC. Analysis of texture in macroradiographs of osteoarthritic knees using the fractal signature. *Phys Med Biol*. 1991;36:709–22.
- Buckland-Wright JC, Lynch JA, Bird C. Microfocal techniques in quantitative radiography: measurement of cancellous bone organization. *Br J Rheumatol*. 1996;35(Suppl 3):18–22.
- Cowin SC. A resolution restriction for Wolff's law of trabecular architecture. *Bull Hosp Jt Dis Orthop Inst*. 1989;49:205–12.
- Rubin CT, McLeod KJ, Bain SD. Functional strains and cortical bone adaptation: epigenic assurance of skeletal integrity. *J Biomech*. 1990;23(Suppl 1):43–54.
- Khosrovi PM, Kahn AJ, Majumdar HK, Genant CA. Fractal analysis of dental radiographs to assess trabecular bone structure. *J Dent Res*. 1995;74(Spec. Issue):173 (abstr. 1294).
- Ruttiman UE, Ship JA. The use of fractal geometry to quantitate bone structure from radiographs. *J Dent Res*. 1990;69(Spec. Issue):287 (abstr. 1431).
- Van Der Stelt PF, Geraets WGM. Use of the fractal dimension to describe the trabecular pattern of osteoporosis. *J Dent Res*. 1990;69(Spec. Issue):287 (abstr. 1430).
- Otis LL, Hong JSH, Tuncay OC. Bone structure effect on root resorption. *Orthod Craniofac Res*. 2004;7:165–77.
- Heo MS, Park KS, Lee SS, Choi SC, Koak JY, Heo SJ, et al. Fractal analysis of mandibular bony healing after orthognathic surgery. *Oral Surg Oral Med Oral Pathol Oral Radiol Endod*. 2002;94:763–7.
- Yasar F, Akgünlü F. The differences in panoramic mandibular indices and fractal dimension between patients with and without spinal osteoporosis. *Dentomaxillofac Radiol*. 2006;35:1–9.
- Prouteau S, Ducher G, Nanyan P, Lemineur G, Benhamou L, Courteix D. Fractal analysis of bone texture: a screening tool for stress fracture risk? *Eur J Clin Invest*. 2004;34:137–42.
- Lee DH, Ku Y, Rhyu IC, Hong JU, Lee CW, Heo MS, et al. A clinical study of alveolar bone quality using the fractal dimension and the implant stability quotient. *J Periodontal Implant Sci*. 2010;40:19–24.
- Branemark P, Zarb GA, Alberktsson T. Tissue integrated prostheses: osseointegration in clinical dentistry. 1st ed. Chicago: Quintessence Publishing; 1985.
- Lundahl T, Ohely WS, Kay SM, Siffert R. Fractional brownian motion: a maximum likelihood estimator and its application to imaging texture. *IEEE Trans Med Imaging*. 1986;5:152–61.
- White SC, Rudolph DJ. Alterations of the trabecular pattern of the jaws in patients with osteoporosis. *Oral Surg Oral Med Oral Pathol Oral Radiol Endod*. 1999;88:628–35.
- Chen SK, Ovir T, Lin CH, Leu LJ, Cho BH, Hollender L. Digital imaging analysis with mathematical morphology and fractal dimension for evaluation of periapical lesions following endodontic treatment. *Oral Surg Oral Med Oral Pathol Oral Radiol Endod*. 2005;100:467–72.
- Lynch JA, Hawkes DJ, Buckland-Wright JC. A robust and accurate method for calculating the fractal signature of texture in macroradiographs of osteoarthritic knees. *Med Inform*. 1991;16:241–51.
- Fortin C, Kumaresan R, Ohley W, Hoffer S. Fractal dimension in the analysis of medical images. *IEEE Eng Med Biol Mag*. 1992;11:65–71.
- Ruttiman UE, Webber RL, Hazelrig JB. Fractal dimension from radiographs of periodontal alveolar bone. A possible diagnostic indicator of osteoporosis. *Oral Surg Oral Med Oral Pathol*. 1992;74:98–110.
- Gatz D, Ehrlich J, Kohen Y, Bab I. Effect of occlusal (mechanical) stimulus on bone remodelling in rat condyle. *J Oral Pathol*. 1987;16:395–8.

25. Feik SA, Storey E, Ellender G. Stress induced periosteal changes. *Br J Exp Pathol.* 1987;68:803–13.
26. Rubin CT, Lanyon LC. Regulation of bone formation by applied dynamic loads. *Calcif Tiss Int.* 1985;37:411–7.
27. Cowin SC, Sadegh AM, Luo GM. An evolutionary Wolff's law for trabecular architecture. *J Biomech Eng.* 1992;114:129–36.
28. Weinans H, Huijskes R, Grootenboer HJ. The behavior of adaptive bone-remodeling simulation models. *J Biomech.* 1992;25:1425–41.
29. Chambers TJ, Evans M, Gardner TN, Turner-Smith A, Chow JW. Induction of bone formation in rat tail vertebrae by mechanical loading. *Bone Miner.* 1993;20:167–78.
30. Caldwell CB, Stapleton SJ, Holdsworth DW, Jong RA, Weiser WJ, Cooke G, et al. Characterization of mammographic parenchymal pattern by fractal dimension. *Phys Med Biol.* 1990;35:235–47.
31. Aldell R, Lekholm U, Rockler B, Brånemark PI. A 15 year study of osseointegrated implants in the treatment of the edentulous jaw. *Int J Oral Surg.* 1981;10:387–416.
32. Quirynen M, Naert I, van Steenberghe D. Fixture design and overload influence on marginal bone loss and fixture success in the Branemark implants system. *Clin Oral Implants Res.* 1992;3:104–11.
33. Albrektsson T, Zarb GA, Worthington P, Eriksson AR. A positive correlation between occlusal trauma and periimplant bone loss: a review and proposed criteria of success. *Int J Oral Maxillofac Implants.* 1986;1:11–25.
34. Shrout MK, Potter BJ, Hildebold CF. The effect of image variations on fractal dimension calculations. *Oral Surg Oral Med Oral Pathol Oral Radiol Endod.* 1997;84:96–100.
35. Shrout MK, Potter BJ, Hildebold CF. The effect of image variations on fractal dimension calculations of fractal index. *Dentomaxillofac Radiol.* 1997;26:295–8.
36. Majumdar S, Weinstien RS, Prasad RR. Application of fractal geometry techniques to the study of trabecular bone. *Med Phys.* 1993;20:1611–9.
37. Wilding RJC, Slabbert JCG, Kathree H, Owen CP, Crombie K. The use of fractal analysis to reveal remodeling in human alveolar bone following the placement of dental implants. *Arch Oral Biol.* 1995;40:61–72.
38. Bollen AM, Taguchi A, Hugoel PP, Hollender LG. Fractal dimension on dental radiographs. *Dentomaxillofac Radiol.* 2001;30:270–5.
39. Shrout MK, Hildebold CF, Potter BJ, Comer RW. Comparison of 5 protocols based on their abilities to use data extracted from digitized clinical radiographs to discriminate between patients with gingivitis and periodontitis. *J Periodontol.* 2000;71:1750–5.
40. Schepers HE, van Beek JHGM, Bassingthwaighte JB. Four methods to estimate the fractal dimension from self-affine signals. *IEEE Eng Med Biol Mag.* 1992;11:57–64.
41. Law AN, Bollen AM, Chen SK. Detecting osteoporosis using dental radiographs: a comparison of 4 methods. *J Am Dent Assoc.* 1996;127:1734–42.
42. Yasar F, Akgünlü F. Fractal dimension and lacunarity analysis of dental radiographs. *Dentomaxillofac Radiol.* 2005;34:261–7.
43. Ergün S, Saraçoğlu A, Güneri P, Özpınar B. Application of fractal analysis in hyperparathyroidism. *Dentomaxillofac Radiol.* 2009;38:281–8.
44. Nair MK, Seyedain A, Webber RL, Nair UP, Piesco NP, Agarwal S, et al. Fractal analyses of osseous healing using tuned aperture computed tomography images. *Eur Radiol.* 2001;11:1510–5.
45. Southard TE, Southard KA, Jakobsen JR, Hillis SL, Najin CA. Fractal dimension in radiographic analysis of alveolar bone. *Oral Surg Oral Med Oral Pathol Oral Radiol Endod.* 1996;82:569–76.
46. Caligiuri P, Giger ML, Favus M. Multifractal radiographic analysis of osteoporosis. *Med Phys.* 1994;21:503–8.
47. Misch CE, Qu M, Bidez MW. Mechanical properties of trabecular bone in the human mandible: implication of dental implant treatment planning and surgical placement. *J Oral Maxillofac Surg.* 1999;57:700–6.
48. Thomsen JS, Ebbesen EN, Mosekilde L. Relationships between static histomorphometry and bone strength measurements in human iliac crest bone biopsies. *Bone.* 1998;22:153–63.
49. Roberts WE, Turley PK, Brezniak N, Fielder PJ. Implants: bone physiology and metabolism. *CDA J.* 1987;15:54–61.
50. Taylor TD. Osteogenesis of the mandible associated with implant reconstruction: a patient report. *Int J Oral Maxillofac Implants.* 1989;4:227–31.
51. von Wowers N, Harder F, Hjorting-Hansen E, Gotfredsen K. ITI implants with overdentures: a prevention of bone loss in edentulous mandible? *Int J Oral Maxillofac Implants.* 1990;5:135–9.
52. Shrout MK, Roberson B, Potter BJ, Mailhot JM, Hildebold CF. A comparison of 2 patient populations using fractal analysis. *J Periodontol.* 1998;69:9–13.
53. Misch CE, Wang HL, Palti A. The International Congress of Oral Implantologists consensus congress on implant success. Italy: Padua; 2007.
54. Misch CE. Divisions of available bone in implant dentistry. *Int J Oral Implantol.* 1990;7:9–17.
55. Trisi P, Rao W. Bone classification: clinical-histomorphometric comparison. *Clin Oral Implants Res.* 1999;10:1–7.
56. Friberg B, Sennerby L, Roos J, Johansson P, Strid CG, Lekholm U. Evaluation of bone density using cutting resistance measurements and microradiography: an in vitro study in pig ribs. *Clin Oral Implants Res.* 1995;6:164–71.
57. Rosenthal DI, Ganott MA, Wyshak G, Slovik DM, Doppelt SH, Neer RM. Quantitative computed tomography for spinal density measurement: factors affecting precision. *Invest Radiol.* 1985;20:306–10.
58. Norton MR, Gamble C. Bone classification: an objective scale of bone density using the computerized tomography scan. *Clin Oral Implants Res.* 2001;12:79–84.
59. Pouilles JM, Tremolieres F, Todorovsky N, Ribot C. Precision and sensitivity of dual-energy X-ray absorptiometry in spinal osteoporosis. *J Bone Miner Res.* 1991;6:997–1002.